

# We are IntechOpen, the world's leading publisher of Open Access books Built by scientists, for scientists

6,900

Open access books available

186,000

International authors and editors

200M

Downloads

Our authors are among the

154

Countries delivered to

TOP 1%

most cited scientists

12.2%

Contributors from top 500 universities



WEB OF SCIENCE™

Selection of our books indexed in the Book Citation Index  
in Web of Science™ Core Collection (BKCI)

Interested in publishing with us?  
Contact [book.department@intechopen.com](mailto:book.department@intechopen.com)

Numbers displayed above are based on latest data collected.  
For more information visit [www.intechopen.com](http://www.intechopen.com)



# Experimental Investigation of Dynamic Compression and Damage Kinetics of Glass/Epoxy Laminated Composites under High Strain Rate Compression

Tarfaoui Mostapha

*ENSIETA /MSN, 2, rue François Verny, 29806 Brest cedex 9  
France*

## 1. Introduction

The choice of composite materials as a substitute for metallic materials in high technological applications such as in the marine field is becoming more pronounced especially due to the great weight-savings these materials offer. In many of these practical situations, the structures are subjected to high impact loads like slamming, impact, underwater explosions or blast effects. Material and structural response vary significantly under impact loading conditions compared to static loading. The mechanical characteristics of these materials are well known for static loading; however, with the strain rate they are likely to evolve (Goldsmith et al., 1995; Shi et al., 1993; Tsai & Sun, 2004; Tsai & Sun, 2005; Gillespie et al., 2005; Brara & Klepaczko, 2007). The behaviour of structures subjected to impact has been of interest to many scientists for design purposes as well as for the purpose of developing constitutive models of the materials tested [7-8]. The study of the composite materials behaviour at high strain rates is still relatively new and reliable data on strain rate effects is very scarce. Even though the problem of obtaining reliable data is accentuated by difficulties encountered in design and conducting impact tests on composites [9], the qualitative relationship between the dynamic constitutive response and the dynamic damage evolution for composites at high strain rates is still far from being fully understood. To investigate the rate-dependent constitutive relations of materials at high strain rates, the Split Hopkinson Pressure Bar (SHPB) technique has been extensively accepted [10]. Experience of the use of SHPB for the investigation of metals has led to the adaptation of this technique for the characterization of laminated polymer composites at medium strain rates. Significant efforts have been made to examine the high strain rate behaviour of more brittle materials such as composites and ceramics using the split Hopkinson bar to measure dynamic response of materials under varying loading conditions (Kumar et al., 1986); (El-Habak, 1991), (Harding, 1993), (Sierakowski & Nevill, 1971). Ochola et al. (2004) studied the strain rate sensitivity of both carbon fibre reinforced polymer (CFRP) and glass fibre reinforced polymer (GFRP). The results show that the dynamic material strength for GFRP increases with increasing strain rates and the failure strain for both CFRP and GFRP is seen to decrease with increasing strain rates. Vinson & Woldensenbet's (2001) results show that the ultimate stress

increases with increasing strain rate. Most recently, the study conducted by Hosur et al. (2004) presents the effect of in-plane off-axis testing of an 8-harness satin weave carbon fabric/SC15 composite specimen. The specimens were tested in the in-plane direction of  $0^\circ$ ,  $15^\circ$ ,  $30^\circ$ ,  $45^\circ$ ,  $60^\circ$ ,  $75^\circ$ , and  $90^\circ$  in a range of strain rates from 1092 to 2425  $s^{-1}$ . From this study it was noted that the high strain rate-tested specimens showed a considerable increase in the stress to failure and stiffness of the composite compared with the quasistatic loaded specimens. Depending on the fibre orientation of the specimens, the ultimate strength and strain varied considerably and exhibited a nonlinear stress-strain response that increased with angles up to  $45^\circ$ . Gary & Zhao (2000) employed the use of low impedance materials such as nylon, for the incident and output bars of the split Hopkinson bar, to test the strain rate behaviour of glass epoxy composite panels. The failure strength of the glass epoxy panel tested by Gary and Zhao is reported to be strain rate sensitive. Fibre orientation effects on high strain rate properties were considered recently for a carbon epoxy system. Tsai & Sun (2002) have reported the difference between tensile and compressive behaviours in a unidirectional glass fibre-reinforced composite, and developed a nonlinear rate-dependent viscoplasticity model to characterize its compressive stress-strain relationship. Many different models (Gama et al., 2001), (Haque & Ali, 2005), (Vinson. & Woldesenbet, 2001) have been developed to predict failure stress and modes in composites subjected to quasi-static loading. However, few criteria have been developed and experimentally validated for high strain rate loading.

In this study, specimens of glass/epoxy composite were subjected to static and dynamic compression loading. Quasi-static tests were conducted on an Instron universal machine to evaluate the elastic properties and quasi-static response, while the split-Hopkinson pressure bar (SHPB) is used for dynamic tests. Samples were tested in-plane and out of plane direction. The fibre orientations of the samples were  $0^\circ$ ,  $\pm 20^\circ$ ,  $\pm 30^\circ$ ,  $\pm 45^\circ$ ,  $\pm 60^\circ$ ,  $\pm 70^\circ$  and  $90^\circ$ . Stress-strain curves at increasing strain rates were obtained for different cases. However, no experimental data for the intermediate range of strain rates between ( $80s^{-1}$  to  $300s^{-1}$ ) was obtained, because the Instron universal testing machine and the SHPB employed in the experimental tests are designed respectively for low and high strain rates. Off-axis composites and angle-ply laminates exhibited significant nonlinear and strain-dependent behaviour. Finally, experimental observations enable us to draw up a history of dynamic damage in the specimens according to fibre orientation and load direction.

## 2. Materials

The material used in this study consists of 2400 Tex E-glass fibres impregnated with an epoxy matrix. The resin is an EPOLAM pre-polymer, EPOLAM 2020 hardener and 2020 accelerator from Axson. Glass fibres are commonly used for naval applications because of their high strength/mass ratio and their low cost compared to other reinforcements. The reinforcement consists of a plain weave fabric with 90% warp yarns and 10% weft yarns. Panels are made by an infusion process and seven orientations are studied:  $0^\circ$ ,  $\pm 20^\circ$ ,  $\pm 30^\circ$ ,  $\pm 45^\circ$ ,  $\pm 60^\circ$ ,  $\pm 70^\circ$  and  $90^\circ$ . The square panels, 500×500 mm, were cut into cubic samples of the geometry dimensions as shown in Table 1. The standard deviations are indicated in brackets.

Panel	Thickness, (mm)	Surface (mm <sup>2</sup> )	Void fraction (%)	Stacking sequence	Fibre volume Fraction (%)
A	13.00 (0.1)	13×13 (0.2)	2.26	[0] <sub>40</sub>	53.5 (0.5)
B	12.52 (0.3)	13×13 (0.2)	2.00	[±20] <sub>20</sub>	54.0 (0.5)
C	13.00 (0.1)	13×13 (0.2)	1.78	[±30] <sub>20</sub>	55.0 (0.5)
D	12.78 (0.2)	13×13 (0.2)	1.69	[±45] <sub>20</sub>	54.3 (0.5)

Table 1. Geometry and fibre mass fraction of the samples, standard deviation in brackets

Two types of static compression tests are used to obtain the elastic properties of the lamina. In-plane loading (IP), parallel to the plies plane; plane (1,2), and out-of-plane loading (OP), according to the thickness; direction 3 (Figure 1). Table 2 compares the elastic values of the characteristics drawn from relations of micromechanics (Chamis, 1984) with those resulting from experimental work.

Characteristics	E <sub>1</sub> (MPa)	E <sub>2</sub> (MPa)	E <sub>3</sub> (MPa)	v <sub>12</sub>	v <sub>13</sub>	v <sub>23</sub>	G <sub>12</sub> (MPa)	G <sub>13</sub> (MPa)	G <sub>23</sub> (MPa)
Experimental	46217	16086	9062	0.28	0.41	0.097	2224	3500	4540
Rules law	42030	14524	9130	0.31	-	0.01	3441	3273	4508

Table 2. Elastic properties of E-glass/epoxy lamina

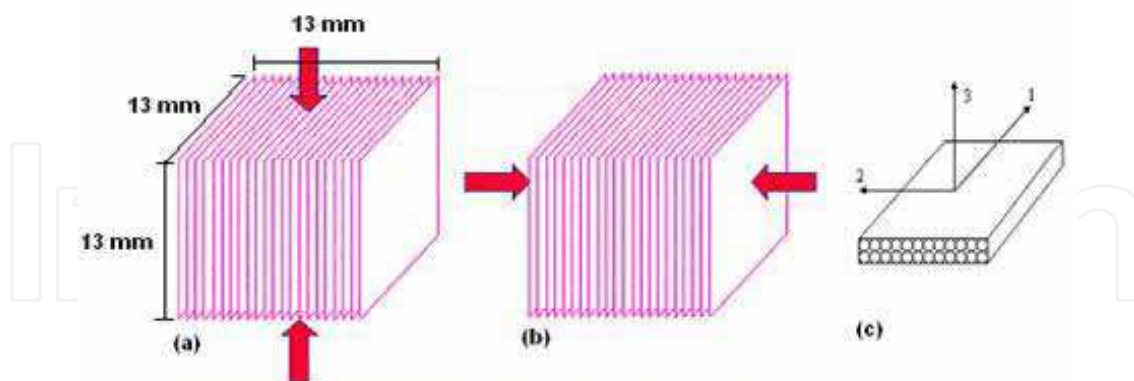


Fig. 1. Sample loadings and coordinates of axis

### 3. Dynamic compression loading

The split Hopkinson bar test is the most commonly used method for determining material properties at high strain rates, Figure 2. This technique of characterization, based on the response of material to wave propagation for high strain rate, was improved by Kolsky (1949).

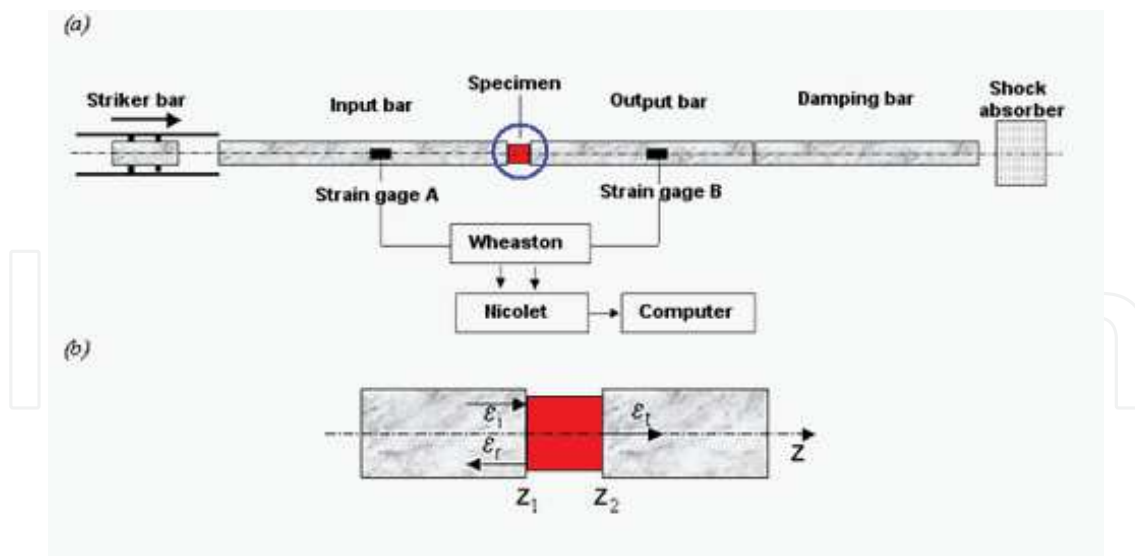


Fig. 2. Typical compressive split Hopkinson bar apparatus

### 3.1 Assumption for description of material deformation

We assume for the mathematical description of material deformation under dynamic impact (Zukas et al., 1992):

1. The state of the stress over the cross-sectional area is one-dimensional and uniaxial.
2. The state of the stress at any instant is homogenous and in equilibrium over the entire composite specimen.
3. Transverse strain, lateral inertia, and body forces are negligible.
4. Frictions with the interfaces bar-sample are negligible.

A wave is dispersive if it changes shape (through components which travel at different velocities). Issues related to the effect of dispersion in a SHPB at a high strain rate are worthy of verification because composite materials undergo elastic deformation under dynamic or non-uniform loading conditions, making it possible for the pulse to change in amplitude and duration during transmission through the specimen. Since the calculated axial stress in the specimen depends linearly on the axial strain on the output bar, wave dispersion would result in underestimating the strength of the specimen.

Using longer bars and a short specimen minimizes the effect of non-uniform stress and non-equilibrium within the specimen used in this study. Since the time to traverse the specimen is short compared to the duration of the wave, equilibrium within the specimen is satisfied by the possible multiple reflections, (Ravichandran & Subbash, 1994). Thus, stress will be homogenous within the specimen, satisfying assumption (3). Transverse strain, lateral inertia, and body forces are all negligible since the rise time condition is satisfied and the impact is parallel to the longitudinal direction. Validity of the SHPB for application to the dynamic behaviour of materials is well documented (Zhao & Gary, 1996), (Follansbee & Frantz, 1983).

### 3.2 Stress, strain and strain rate in the specimen

Dynamic loading of the composite panels is provided by a SHPB for compression tests. The longitudinal impact load  $F_0$  of the striker generates the uniaxial stress pulse transmitted to the input bar as:

$$\sigma(t) = \frac{F_0}{S_b} = (\rho c_0) V_p(t) \tag{1}$$

$c_0$  is the velocity of the wave pulse, bars of  $S_b$  is the bars cross-section area,  $V_p(t)$  the particle velocity, and  $\rho$  the density of the striker material. Accurate measurements of the wave pulse and particle velocity in dynamic impact studies are important since the wave pulse is in fact the propagation of the disturbance or vibration of the particles. The amplitude of the incident wave pulse depends on the impact velocity (a function of the applied air pressure) and material properties of the striker.

$$\frac{\partial^2 u}{\partial t^2} - c_0 \frac{\partial^2 u}{\partial z^2} = 0 \tag{2}$$

$c_0 = \sqrt{E_0 / \rho}$ ,  $E_0$  is the Young modulus and  $u(z,t)$  the longitudinal displacement. The solution yields:

$$\frac{\partial u}{\partial z} = \frac{\alpha}{c_0} \cdot \frac{\partial u}{\partial t} \tag{3}$$

$\alpha = -1$  for wave propagation in the positive direction,  $\alpha = 1$  for the wave propagation in the negative direction. It leads to solutions:  $u = u(z - c_0 t)$  for  $\alpha = -1$  and  $u = u(z + c_0 t)$  for  $\alpha = 1$ .

The particle velocity is as follow:

$$V_p(z,t) = \frac{\partial u(z,t)}{\partial t} \tag{4}$$

Velocities with the interfaces specimen/bars are:  $V_1 = \frac{dZ_1}{dt}$  and  $V_2 = \frac{dZ_2}{dt}$ .

where  $Z_1 = z_1 + u(z_1,t)$  and  $Z_2 = z_2 + u(z_2,t)$

With the deformation, the length of the specimen is  $L = Z_2 - Z_1 = u(z_2,t) - u(z_1,t) + L_0$

where  $L_0 = z_2 - z_1$ . Then:

$$L = L_0 - \int_0^t (V_2 - V_1) dt \tag{5}$$

Equations (6) and (7) give respectively, the strain, the stress and the strain rate in the sample.  $\epsilon_i$ ,  $\epsilon_r$ ,  $\epsilon_t$  being respectively the incidental and reflected deformations pulse at the input bar/specimen interface and that transmitted by the interface specimen/output bar interface, Figure 1b. Those are determined by transport formulas of the signals of the gauges towards the interfaces specimen/bars. This transport takes into account the correction of the dispersive character of the propagation, of the deformations pulse in the bars, by optimization of the decomposition coefficients, in series of Fourier, of the signals. The particles in the input bar will propagate to the right at a relative velocity of  $V_b$  in the longitudinal direction of the wave pulse. With a specimen of cross-sectional area  $S_0$ ,

sandwiched between the input and output bars, equilibrium at the interfaces is satisfied by the continuities of forces and velocities at the interfaces such that the particle velocities, sample stress, strain and strain rate for a thin sample are derived as:

$$V_s = V_t - (V_i + V_r) \text{ with } \begin{cases} V_i = -c_0 \cdot \epsilon_i \\ V_r = c_0 \cdot \epsilon_r \\ V_t = -c_0 \cdot \epsilon_t \end{cases} \rightarrow V_s = -c_0 [\epsilon_t + \epsilon_r - \epsilon_i] = -2c_0 \epsilon_r \quad (6)$$

Assuming equilibrium in short specimen,  $\epsilon_t = \epsilon_i + \epsilon_r$ ; the strain, strain rate and stress is:

$$\begin{aligned} \epsilon_s &= -\frac{2c_0}{L_0} \int_0^t \epsilon_r(t) dt \\ \frac{d\epsilon_s}{dt} &= -\frac{2c_0}{L_0} \epsilon_r(t) \\ \sigma_s &= \frac{S_b}{S_0} E_0 \epsilon_t(t) \end{aligned} \quad (7)$$

### 3.3 Data processing procedure

The dynamic compression test conducted in this study consists in placing a cubic sample (13mm in length) between two bars with a high elastic limit, called input bar and output bar. The bar diameter was 20mm. The striker bar was 0.8m long, while the incident bar length was 3m and the transmission bar 2m. These bars are correctly aligned and are able to slide freely on their support. The composite specimen is not attached to the bar in order to prevent the perturbations of measurements due to additional interfaces. The experimental set-up consists of (1) a stress generating system which is comprised of a split Hopkinson bar and the striker, (2) a specimen, (3) a stress measuring system made up of sensors (typically, resistance strain gauges), and (4) a data acquisition and analysis system. The signals are treated with Maple Software using Fast Fourier Transformation to obtain the evolution of the dynamic parameters: stress vs. strain, strain rate vs. time, incident and transmitted load and velocity at the interfaces input bar/sample and output bar/sample vs. time.

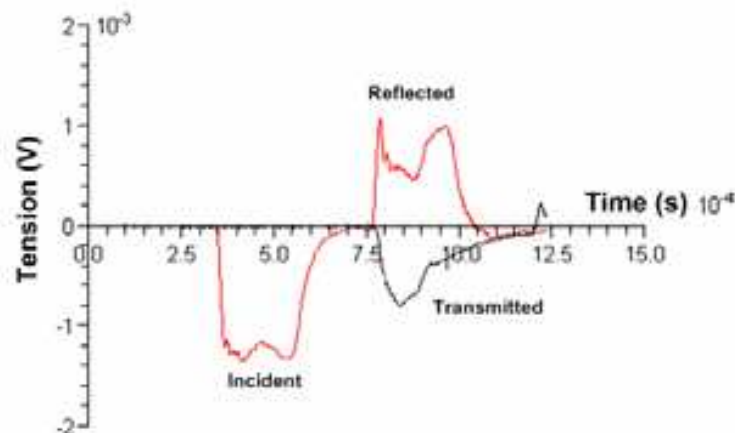


Fig. 3. Typical incident, reflected and transmitted pulse,  $[\pm 60]_{20}$  IP test,  $P=0.9$  bar

The specimens  $[0]_{40}$ ,  $[\pm 20]_{20}$ ,  $[\pm 30]_{20}$ ,  $[\pm 45]_{20}$ ,  $[\pm 60]_{20}$ ,  $[\pm 70]_{20}$  and  $[90]_{40}$  were subjected to the in-plane (IP) and out of plane (OP) loading with nine different impact pressures of the striker bar on the input bar: 0.5, 0.6, 0.7, 0.8, 0.9, 1.0, 1.2, 1.4 and 1.6 bar. A typical set of incident, reflected, and transmitted signals resulting from gauges A and B recorded by the digital oscilloscope from a SHPB experiment on the composite at the strain rate of  $831 \text{ s}^{-1}$  for  $60^\circ$  IP test is shown in figure 3.

#### 4. Dynamic response

Before launching the experimental study for a dynamic case, it is necessary to ensure that the tests can be reproduced. With this objective in mind, for each fibre orientation, a minimum of three tests were carried out at the same impact pressure in order to analyze the tests reproducibility. As figure 4a shows, it is noted that the tests are repeatable and a fact that was checked for each test. Figures 4b and 4c show the velocities and the loads at two faces of specimen. For in-plane and out of plane tests, results for compressive strain rates between  $200 \text{ s}^{-1}$  and  $2000 \text{ s}^{-1}$  are obtained using SHPB. Figure 4d shows the evolution of the strain rate versus time. The maximum value is taken into account for the analysis of the experimental results.

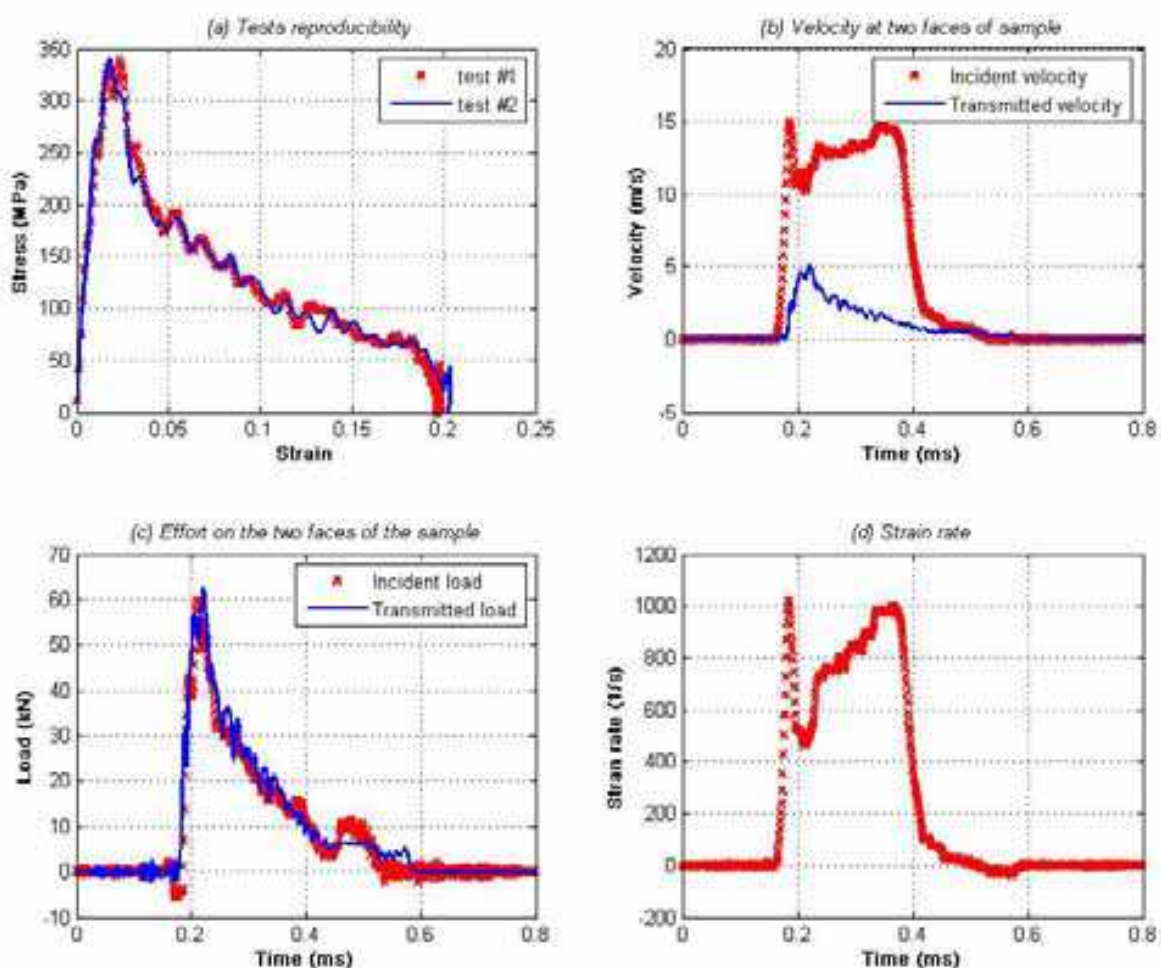


Fig. 4. Test reproducibility, IP test for  $[\pm 30]_{20}$ ,  $P=1.2$  bar

### 4.1 For in-plane tests

The strain rate evolution is sensitive to the entry pressure  $P$  in the chamber of compressed air (impact pressure of the striker on the input bar), the loading direction and the sample lay-up (angle  $\theta$ ). The fibre orientation has an effect on the strain rate evolution. Figure 5 gives an example of the evolution of the strain rate vs. time of  $[0^\circ]_{40}$ ,  $[\pm 20^\circ]_{20}$ ,  $[\pm 30^\circ]_{20}$ ,  $[\pm 45^\circ]_{20}$ ,  $[\pm 60^\circ]_{20}$ ,  $[\pm 70^\circ]_{20}$  and  $[90^\circ]_{40}$ . The presence of a second peak is the principal characteristic of these curves, which characterizes the onset of macroscopic damage, which we will see in detail in section 5. The critical pressure  $P_c$  responsible for the appearance of a second peak is shown in table 3. The appearance of a second peak is around 1.4bar for  $[0^\circ]_{40}$  and between 0.6-0.9bar for the other orientations.

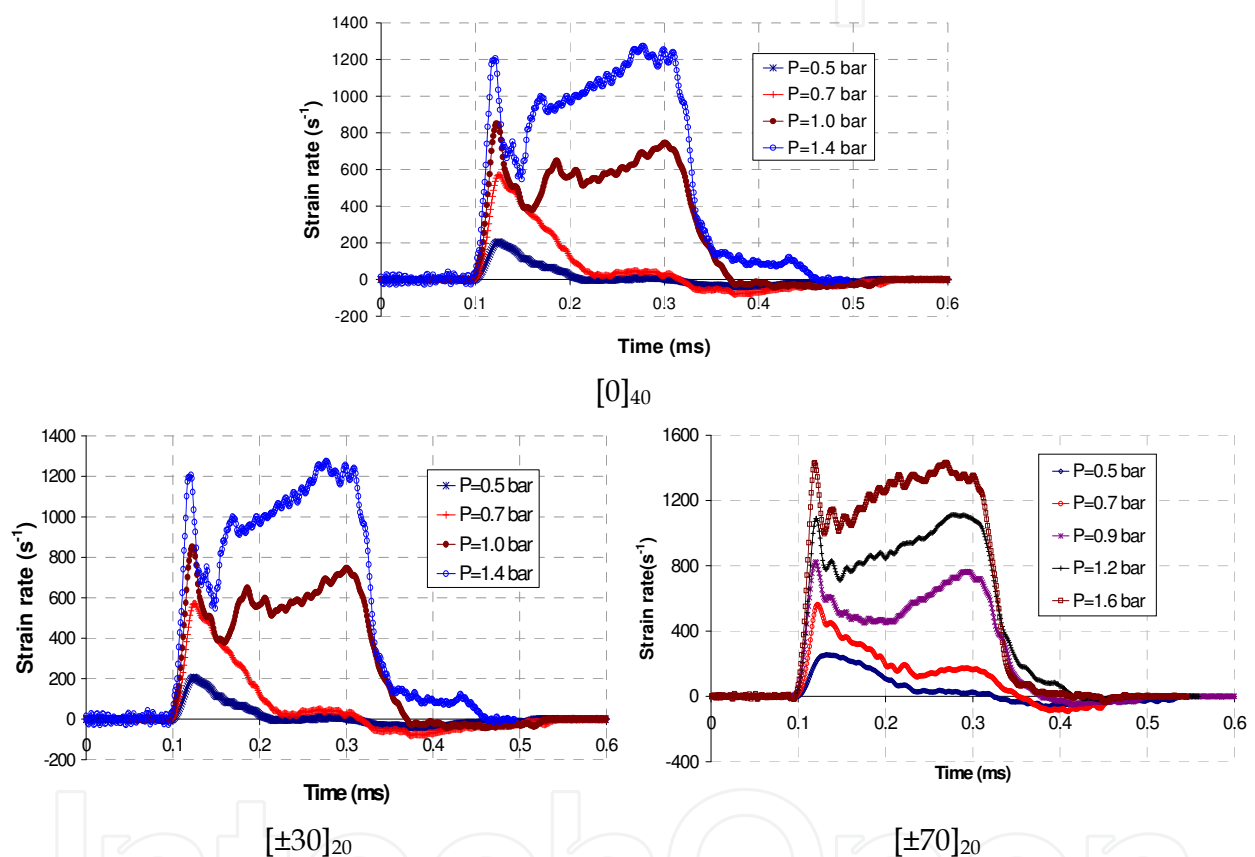


Fig. 5. Strain rate versus impact pressure and stress-strain curve evolution, IP test

IP Tests	0°	±20°	±30°	±45°	±60°	±70°	90°
Pc (bar)	1.2-1.4	0.9	0.8-0.9	0.8	0.7-0.8	0.7	0.6

Table 3. Critical impact pressure for appearance of second peak

The dynamic behaviour for IP tests is dominated by compressive properties of the polymeric matrix and the damage kinetics is affected by fibre orientation. For non damaging tests, the fall of strain rate reaches negative values, which correspond to the springback in the sample. The combination of  $\epsilon = f(t)$  and  $\sigma = f(t)$  curves, which will be discussed in the next paragraph, reveals that the second peak corresponds to the fall of stress in the

sample. The glass/epoxy composite materials present a high strength on compressive dynamic loading for out-of-plane tests (Bancroft, 1941).

Figure 6 shows the dynamic behaviour of the laminates for the 9-impact pressure. One can note that couple  $[\pm 20^\circ]_{20}$ - $[\pm 30^\circ]_{20}$  and  $[\pm 60^\circ]_{20}$ - $[\pm 70^\circ]_{20}$  have similar tendencies. For the  $[90^\circ]_{40}$  laminate, a brittle behaviour is noted, which is controlled by matrix failure. According to the various orientations, the nonlinear part of the  $\sigma = f(\epsilon)$  curves is different and corresponds to different damaging modes.

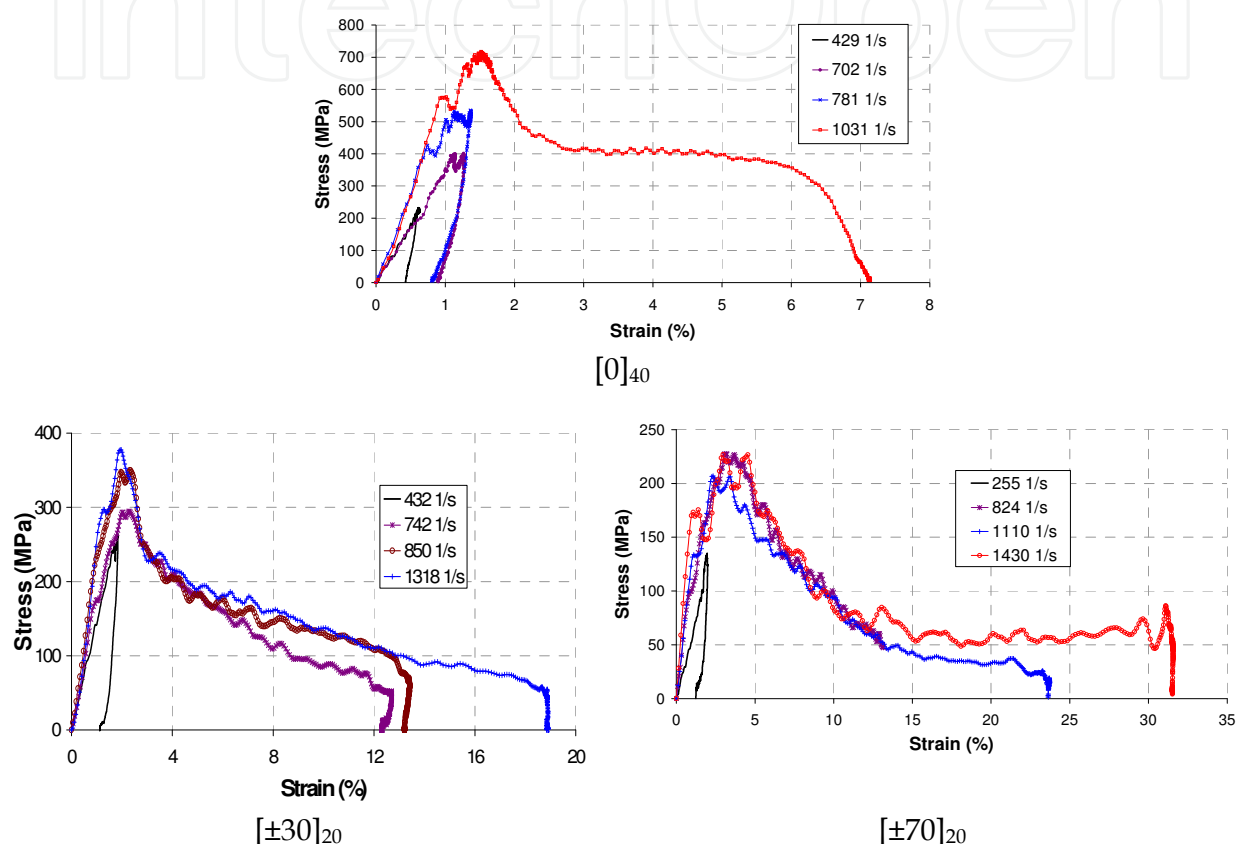


Fig. 6. Strain rate versus impact pressure and stress-strain curve evolution, IP test

With a view to simplifying the graphic representations, the analyzed parameters  $E_{dynamic}$  and  $\sigma_{max}$  will be given according to the impact pressure (P) and the fibre orientation  $\theta$  (Teta). Figure 7 shows the detailed trends of dependencies of  $E_{dynamic}$  and  $\sigma_{max}$  on both fibre orientation and impact pressure. At a given impact pressure, the origin stiffness evolution with fibre orientation presents a minimum around  $55^\circ$ - $65^\circ$ . This tendency is not encountered in quasi-static loading for which a monotonic decrease associated with the fibre orientation increase of  $0^\circ$  to  $90^\circ$  can be analytically proved. This tendency can be explain by the fact that strain rate is not constant at a given impact pressure, as shown in Figure 8, and viscoelastic effects cannot be neglected. For the various orientations, the laminate stiffness  $E_{dynamic}$  and the maximum stress  $\sigma_{max}$  increase with the impact pressure until a pressure threshold is reached from which the tendency is reversed; i.e. they decrease with the increase of impact pressure. Table 3 gives the pressure thresholds. The thermal softening due to inelastic heat dissipation and damage may explain this behaviour.

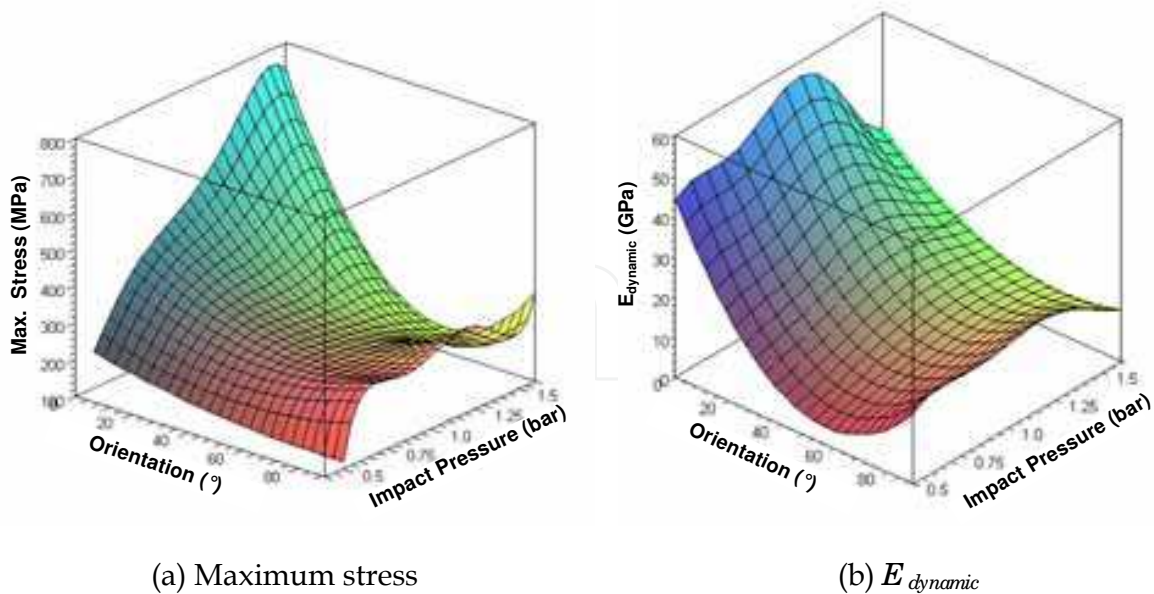


Fig. 7.  $\sigma_{max}$  and  $E_{dynamic}$  versus P and  $\theta$

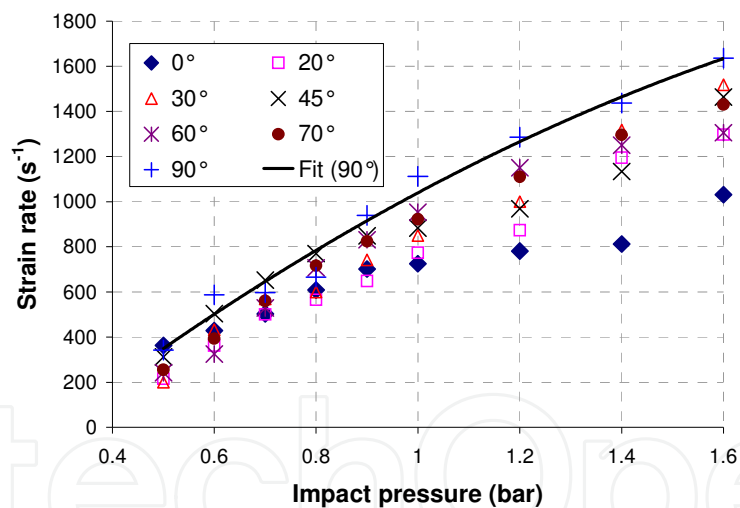


Fig. 8. Strain rate versus impact pressure for different fibre orientations

#### 4.2 For out-of-plane tests

For out-of-plane (OP) tests, figure 8 give the evolution of the strain rate of  $[0^\circ]_{40}$ ,  $[\pm 20^\circ]_{20}$ ,  $[\pm 30^\circ]_{20}$  and  $[\pm 45^\circ]_{20}$  samples for 9 impact pressures. The appearance of a second peak is around 0.9bar for  $[0^\circ]_{40}$  and 1.4bar for the other orientation, Table 4. The dynamic behaviour is dominated by compressive properties of the polymeric matrix and the damage is created for high impact pressure. The fibres orientation affects the initiation and propagation of damage. For undamaging tests, the fall of strain rate passes by negative values, which correspond to the springback in the sample. The glass/epoxy composite materials present a high strength on compressive dynamic loading for OP tests.

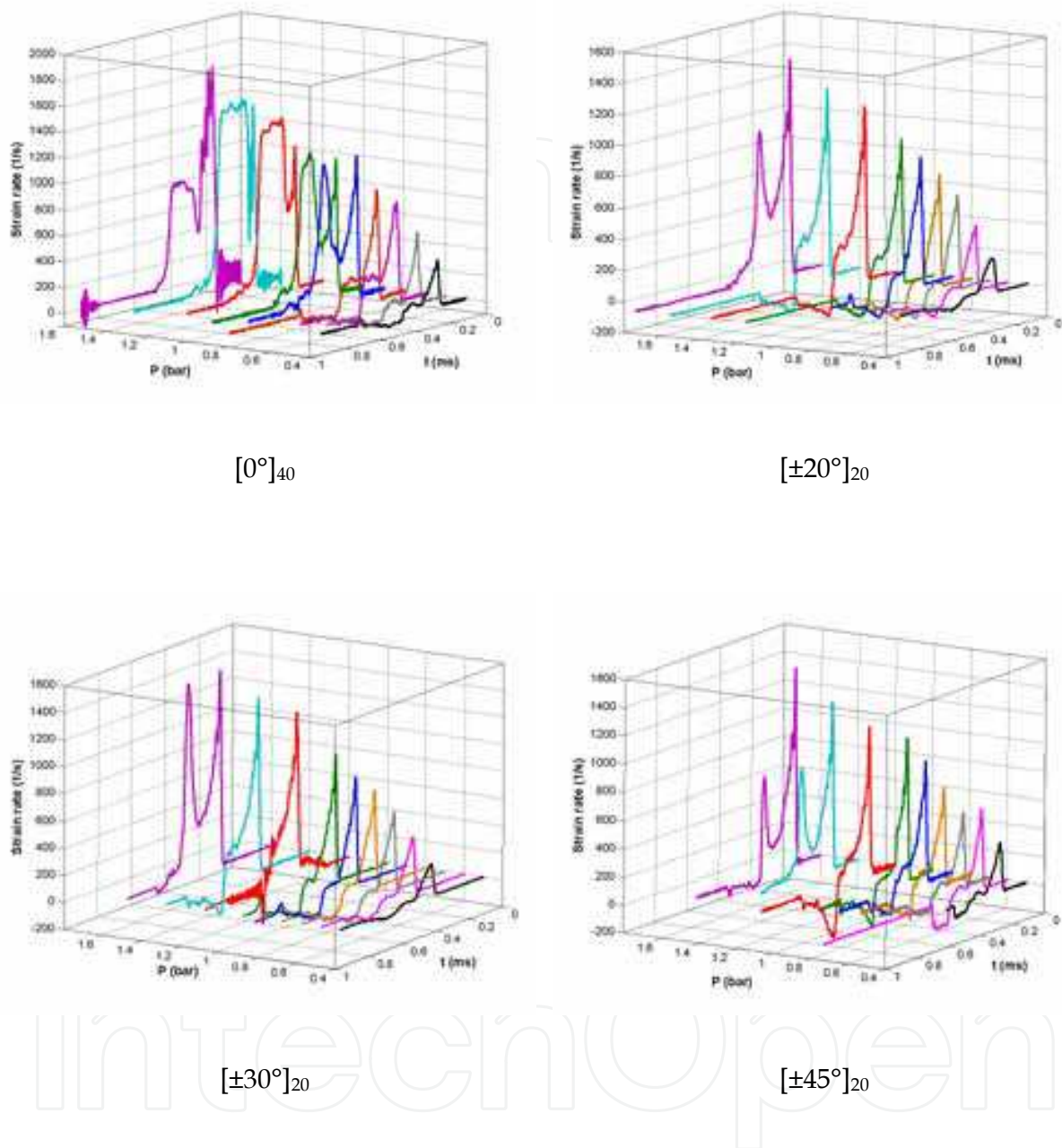


Fig. 9. Strain rate evolution versus impact pressure

OP Tests	$[0^\circ]_{40}$	$[\pm 20^\circ]_{20}$	$[\pm 30^\circ]_{20}$	$[\pm 45^\circ]_{20}$
$P_c$ (bar)	0.9	1.6	1.6	1.4

Table 4. Critical impact pressure for appearance of second peak

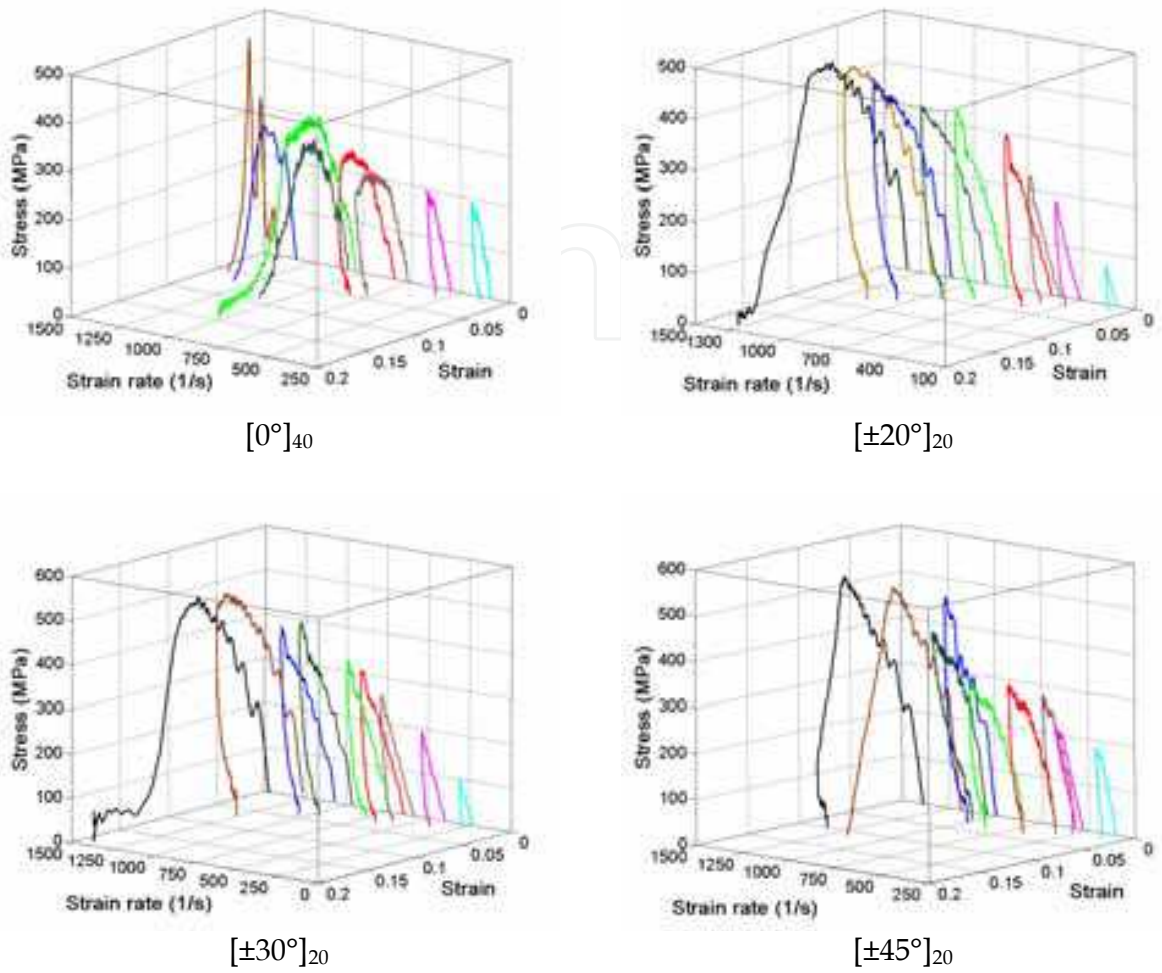


Fig. 10. Stress - Strain curves evolution versus strain rate

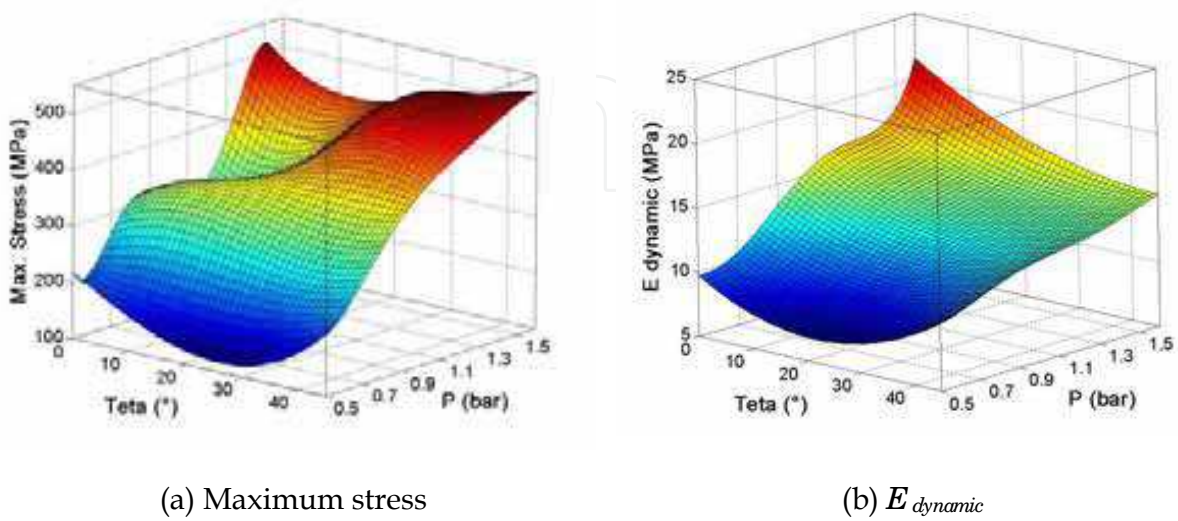


Fig. 11.  $\sigma_{max}$  and  $E_{dynamic}$  versus P and  $\theta$

One can note that [20/70] and [30/60] have similar dynamic response, Figure 10. The unloading part of  $\sigma = f(\epsilon)$  curves indicates if there is plasticity or other damaging modes. The second peak of  $\dot{\epsilon} = f(t)$  curves corresponds to the fall of stress in the sample. The dynamic behaviour of the various laminates is strongly affected by the strain rate and fibres orientation, Figure 11. For OP tests, there is always an increase in  $E_{dynamic}$  and  $\sigma_{max}$  with the increase in the impact pressure. There is not threshold effect for OP loading; the transitional pressure does not exist.

## 5. Kinetics of macroscopic damage

Damage tolerance is an important parameter for the use of composite materials in technologically advanced sectors and in particular for military naval applications. This characterization involves drawing up a history of the damage kinetics of the specimens from initiation to complete failure. Several techniques are used to examine the extent of damage. First, during the dynamic compression high-speed photography and infrared cameras are used to follow the damage in the samples. Frames taken in real time are used to illustrate the evolution of the damage. Impacted samples are inspected by optical techniques and fluorescent dye is applied to improve damage visualization. The onset of macroscopic damage can also be located by the presence of a second peak on the  $\dot{\epsilon} = f(t)$  curve. These various techniques make it possible to follow the macroscopic and microscopic damage. The failure modes preserved in the specimens after mechanical loading at various impact pressures thus well define damage and failure loading history at high impact pressure. According to the results stated previously, it can be concluded that the damaging mode mainly depends on the fibre orientation and the loading direction without significant strain rate effect.

### 5.1 For in-plane tests

Based on the results obtained five damaging modes for  $0^\circ$ ,  $20^\circ$ - $30^\circ$ ,  $45^\circ$ ,  $60^\circ$ - $70^\circ$  and  $90^\circ$  were determined. Figures 12 to 20 summarize the damaging modes for the various laminates. Each figure outlines the specimen's history of damage initiation up to final failure.

In this section we will discuss the damage that occurs in dynamic compression for the various orientations. Through this analysis, we will establish a history of defect development in the samples until final failure.

#### a) For $[0^\circ]_{40}$ laminates

The damage for the  $[0]_{40}$  laminate occurs for an impact pressure higher than 1.4bar ( $\dot{\epsilon} = 845s^{-1}$ ). The damage is initiated by matrix plasticity, which can be detected on the  $\sigma = f(\epsilon)$  curves, Figure 6. It is followed by cracks crossing the layers of the laminate and forming the letter V. The branches of the letter V are due to layer shearing. The shearing mode generates buckling of local layers and matrix cracks. After that, a delamination is initiated with the point of V followed by dilation in the transverse direction that involves a buckling of the external layers. At the end of dynamic compression, this buckling involves a delamination and a separation of several layer blocks. Figure 12 illustrates the evolution of damage.

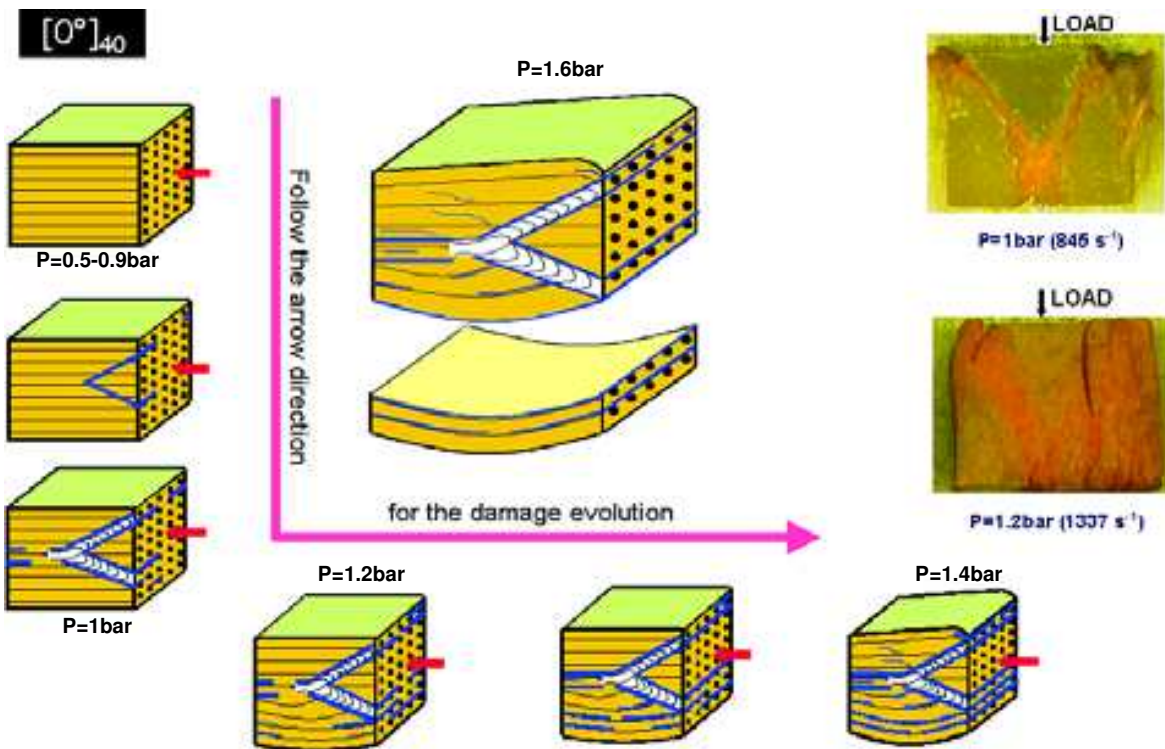


Fig. 12. Damage history of  $[0^\circ]_{40}$  for IP tests at high pressure

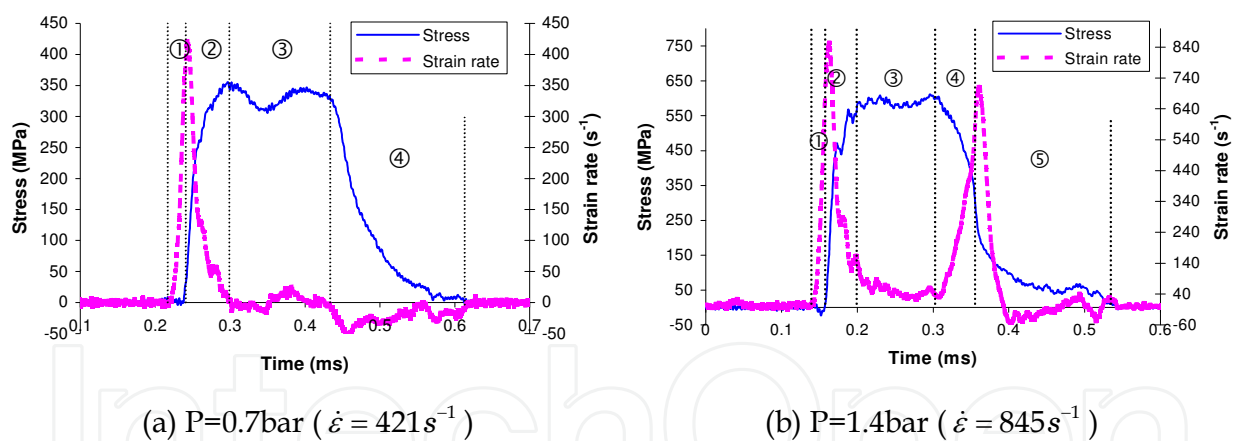


Fig. 13. Strain rate and stress curves for  $[0^\circ]_{40}$

The macroscopic damage can also be detected by the presence of a second peak on the  $\dot{\epsilon} = f(t)$  curve. As shown in figure 13, a fall in stress occurs at the appearance of this peak, which is associated to the formation of the letter V and delamination on the external layers. In the curves describing the strain rate and stress evolution during the test, one can distinguish various zones, which can be summarized as follows:

- i. For non damaging tests, Figure 13a
  - Zone ①: fast evolution of  $\dot{\epsilon}$ , which can be interpreted by the self-installation of the sample between the bars. Indeed, the parallelism of the sample facets in contact with the bars is not 100% guaranteed, which accounts for clearance and zero stress in this zone.

- Zone ②: Once perfect contact is ensured, the strength of material generates a drop in  $\dot{\epsilon}$  and an increase in  $\sigma$ .
- Zone ③: evolution of  $\sigma$  translates the incidental signal evolving around an average value with  $\dot{\epsilon}$  tending towards a zero value. When  $\dot{\epsilon}$  tends towards zero, the sample reaches maximum compression under maximum stress.
- Zone ④: in this zone,  $\dot{\epsilon}$  changes sign whereas  $\sigma$  starts to decrease; the specimen began to relax. This behaviour can be interpreted by the specimen springback, which is carrying out by an analysis of stereotypes taken by high-speed photography. At the end of this zone, the two signals are cancelled at the same time.
- ii. For damaging tests, Figure 13b
  - Zone ① : same observations as for zone 1 of the non damaging tests.
  - Zone ② : Once perfect contact is ensured, material strength generates a drop in  $\dot{\epsilon}$  and an increase in  $\sigma$ .
  - Zone ③ : the stress evolution represents dynamic compression with a constant average value of  $\sigma$  and  $\dot{\epsilon}$ . In this zone, where  $\sigma$  reaches its maximum value, more marked fluctuations compared to the non damaging test. One can explain this phenomenon by the appearance of the damage on a microscopic scale.
  - Zone ④ : the accumulation of microscopic damage involves the appearance of a macroscopic defects. Inherent damage in the specimen generates a rapid fall in the stress with a rapid increase in  $\dot{\epsilon}$ .
  - Zone ⑤: the damaged specimen becomes more compact, which causes a sharp drop in  $\dot{\epsilon}$ . In this zone,  $\sigma$  always decreases but in a way less marked than in zone 4. One can note that the appearance of the damage brings about the disappearance of the springback behaviour.

**b) For  $[\pm 20^\circ]_{20}$  and  $[\pm 30^\circ]_{20}$  laminates**

The impact pressure 0.8bar corresponds to a critical phase where the kinetics of damage evolves differently; this is why the analysis for each laminate will comprise two parts:

i. Pressures lower than 0.8-0.9bar

For this range of pressures,  $[\pm 20^\circ]_{20}$  and  $[\pm 30^\circ]_{20}$  laminates undergo only “plastic deformations” which can be quantified in the same way as for the other laminates by analyzing  $\sigma = f(\epsilon)$  curves. The damage for  $[\pm 30^\circ]_{20}$  laminate appears for lower impact pressures.

ii. Pressures higher or equal to 0.8-0.9bar

- In-plane view

At the beginning, the compression wave generates a deformation on the entire sample. As compression evolves, one can see delamination, which occurs in the opposite sides of the sample. The size and the incidence of this damage become increasingly significant as a result of increasing pressures and they start to cross the sample starting from pressure 1 bar, Figure 14.

- Out-of-plane view

The first damage occurs in the layers plane. Indeed compression generates a crack along the diagonal of the external layers and can sometimes occur along the two diagonals. These cracks can cause the failure of the weft or warp yarns. Figure 14 illustrates the stages of the crack formation along the diagonal.

The same damage history occurs for  $[\pm 20^\circ]_{20}$  and  $[\pm 30^\circ]_{20}$  but the initiation is generated at a high impact pressure for  $[\pm 20^\circ]_{20}$ .

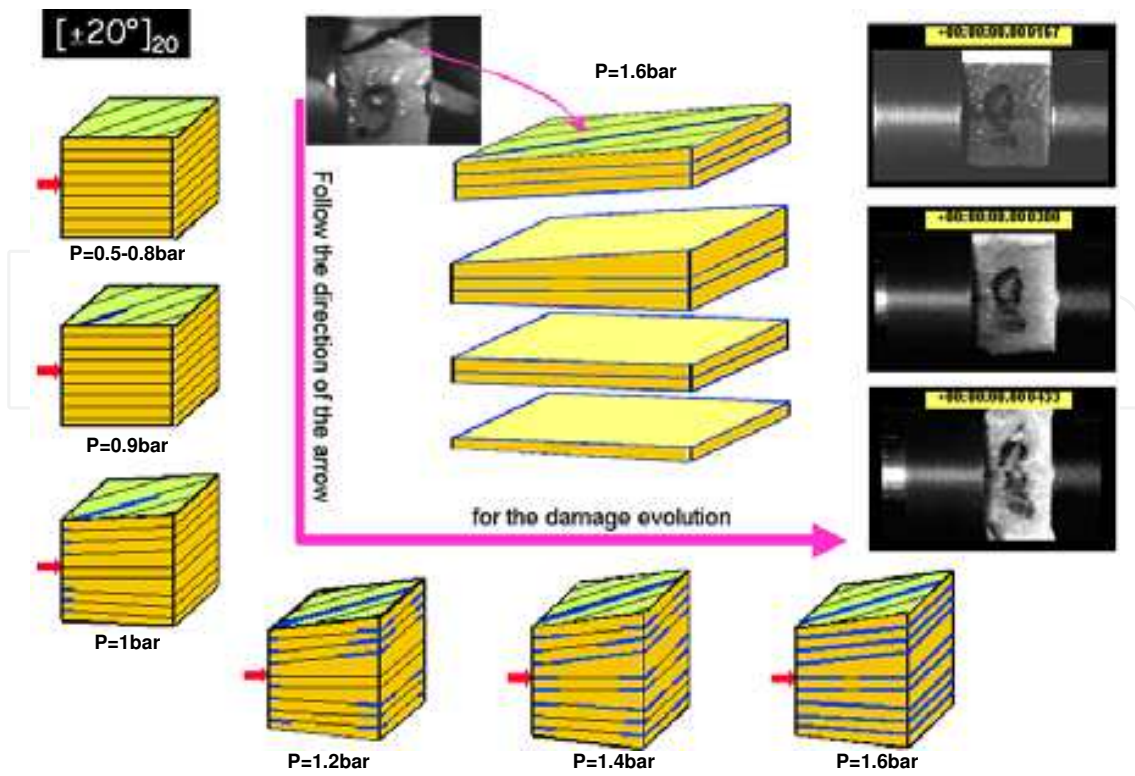


Fig. 14. Damage history of  $[\pm 20^\circ]_{20}$  (and  $[\pm 30^\circ]_{20}$ ) for IP tests at high impact pressure

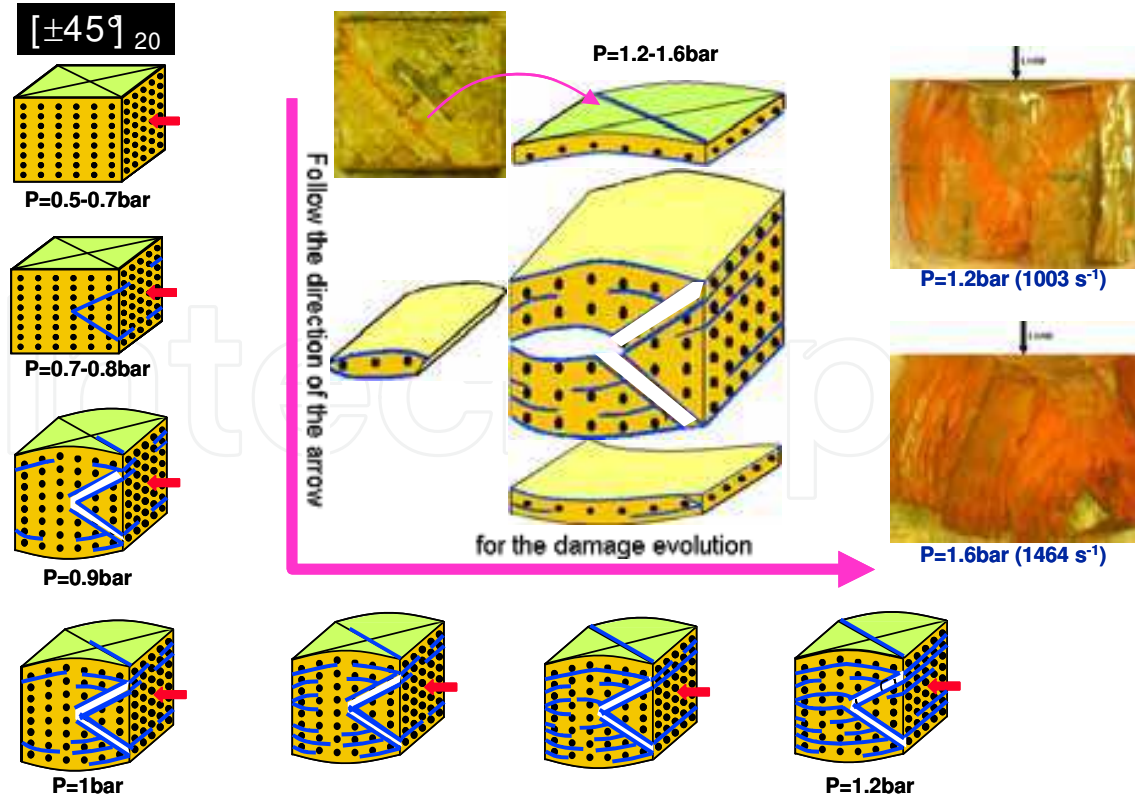


Fig. 15. Damage history of  $[\pm 45^\circ]_{20}$  for IP tests at high impact pressure

**c) For  $[\pm 45^\circ]_{20}$  laminates**

The damage for  $[\pm 45^\circ]_{20}$  laminates occurs for an impact pressure below 0.8bar. The damage is initiated by a crack forming the letter V. This shearing generates local layer buckling and cracks. Compression also generates a crack according to the diagonal of the external layers. The evolution of this compression generates substantial displacement in the thickness direction with a buckling of the external layers. This involves delamination and the final failure is caused by a separation of several layers block, Figure 15.

Figure 16 shows that stress falls with the appearance of a second peak. A comparison of figure 13 and 16 illustrates the difference between  $[0^\circ]_{40}$  and  $[\pm 45^\circ]_{20}$  on dynamic behaviour and damage kinetics. The macroscopic failure is more brittle for  $[0^\circ]_{40}$  than for  $[\pm 45^\circ]_{20}$  since the buckling effect is stronger (higher longitudinal stiffness) for  $[0^\circ]_{40}$  laminates than for  $[\pm 45^\circ]_{20}$  laminates.

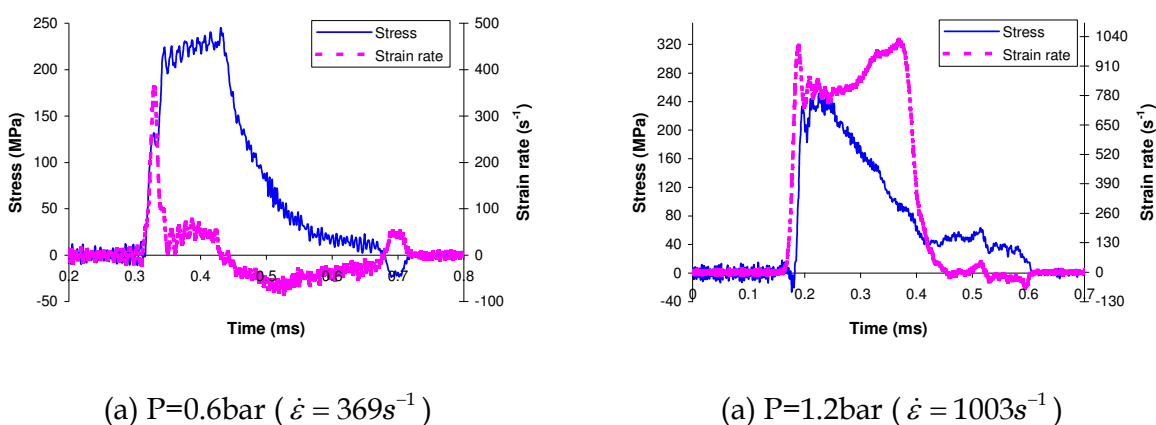


Fig. 16. Strain rate and stress curves for  $[\pm 45^\circ]_{20}$

**d) For  $[\pm 60^\circ]_{20}$  and  $[\pm 70^\circ]_{20}$  laminates**

The damage for  $[\pm 60^\circ]_{20}$  and  $[\pm 70^\circ]_{20}$  laminates occurs for an impact pressure between 0.7 and 0.8 bar.

i. Pressures lower than 0.7-0.8bar

For this impact pressure, slight plastic strain is detected by analyzing the stress-strain curves.

ii. Pressures higher or equal to 0.7-0.8bar

By analyzing the videos and frames it is of note that the dynamic compression of the samples can create three damaging modes independent of the strain rate.

- First damaging mode

The sample undergoes plastic deformation at the beginning of the shock, then compression of the sample generates a damaged zone which has the shape of the letter V on the incidental bar side. The evolution of damage in this zone generates a shearing mode between the V zone and the rest of the specimen. Under the compression wave effect, there is a buckling mode of the external layers, which leads to local delamination at pressures between 0.8 and 1bar. This leads to a delamination of packages of layers for pressures from 1.2 to 1.6bar. At the same time, the penetration of the angular point of V generates delamination of the specimen in the transmitted bar side. Figure 17 shows the stages of damage.

- Second damaging mode

This mode begins with local plasticity followed by the generation of a V zone but on the transmitted bar side. The shearing mode propagates at the tip of the V domain along the two directions formed by the letter V. At the end of this propagation, a large deformation occurs transversally and generates layer buckling under the effect of the compression wave, which causes delamination, and separation of packages of  $n$  layers. Figure 18 illustrates the three stages of the evolution of the damage.

- Third damaging mode

This damaging mode seldom occurs, it begins with a local plasticity, as for the first two previous modes, followed by the formation of two V zones, one on the incidental bar side and the other on the transmitted bar side. This mode is the most severe of the three modes, this is why it can cause extensive damage even at relatively low impact pressures, Figure 19.

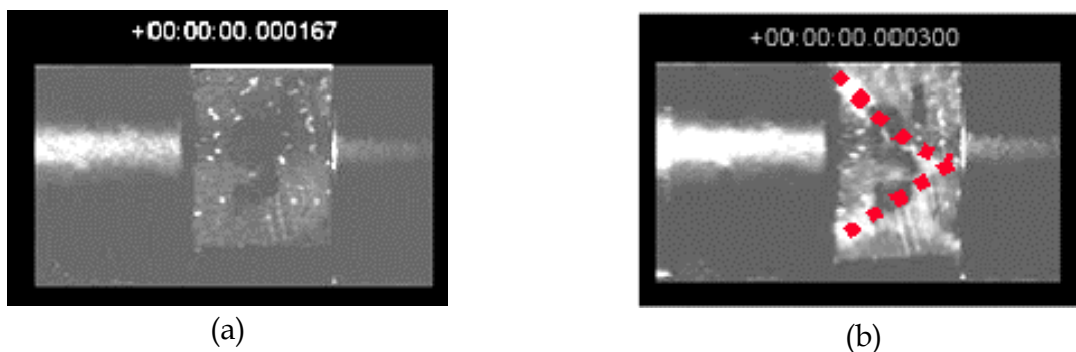


Fig. 17. First damaging mode of  $[\pm 60^\circ]_{20}$  for in-plane tests

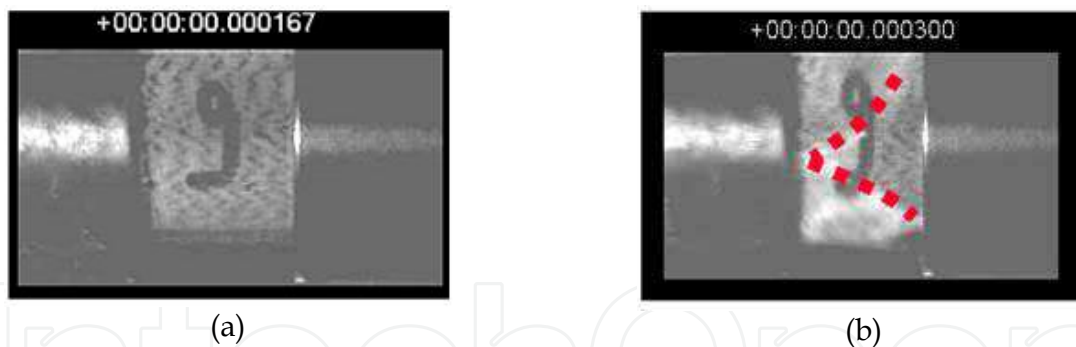


Fig. 18. Second damaging mode of  $[\pm 60^\circ]_{20}$  for in-plane tests

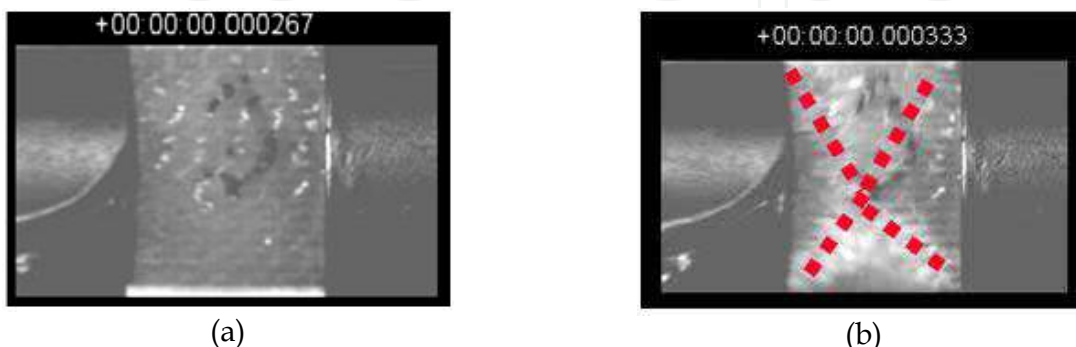


Fig. 19. Third damaging mode of  $[\pm 60^\circ]_{20}$  for in-plane tests

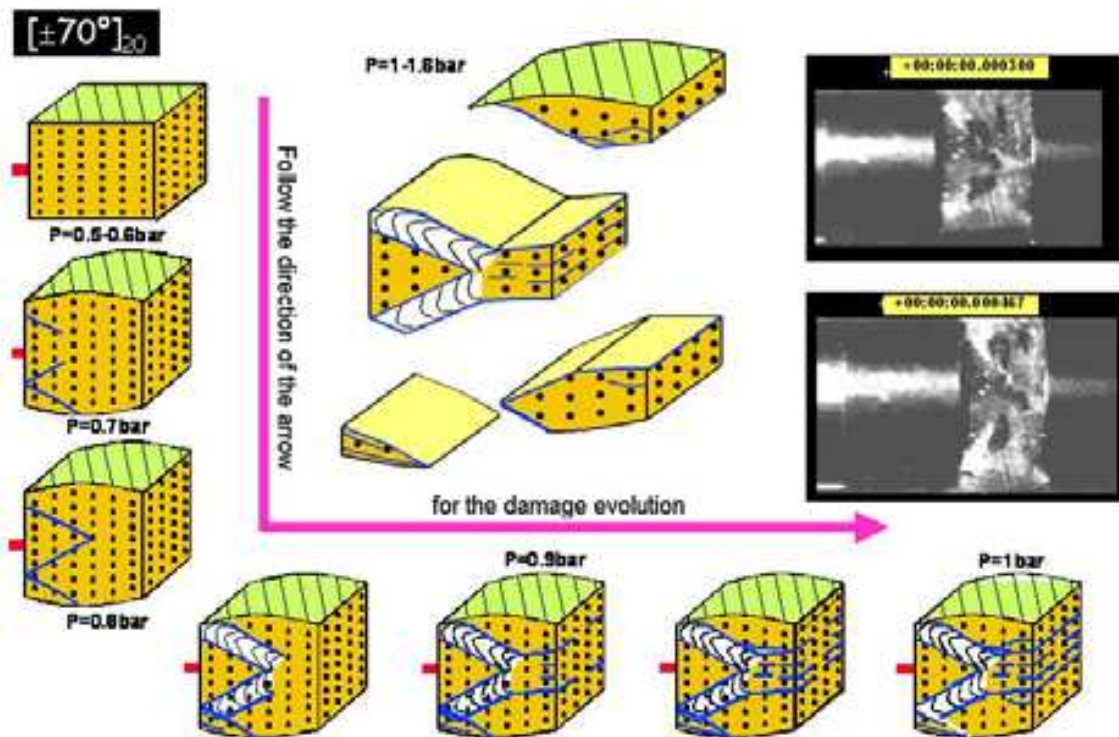


Fig. 20. Damage history of  $[\pm 70^\circ]_{20}$  for IP tests at high impact pressure

The same damage history occurs for  $[\pm 60^\circ]_{20}$  and  $[\pm 70^\circ]_{20}$  but the fragments of the  $[\pm 70^\circ]_{20}$  laminates are larger and there are few delamination modes, Figure 20.

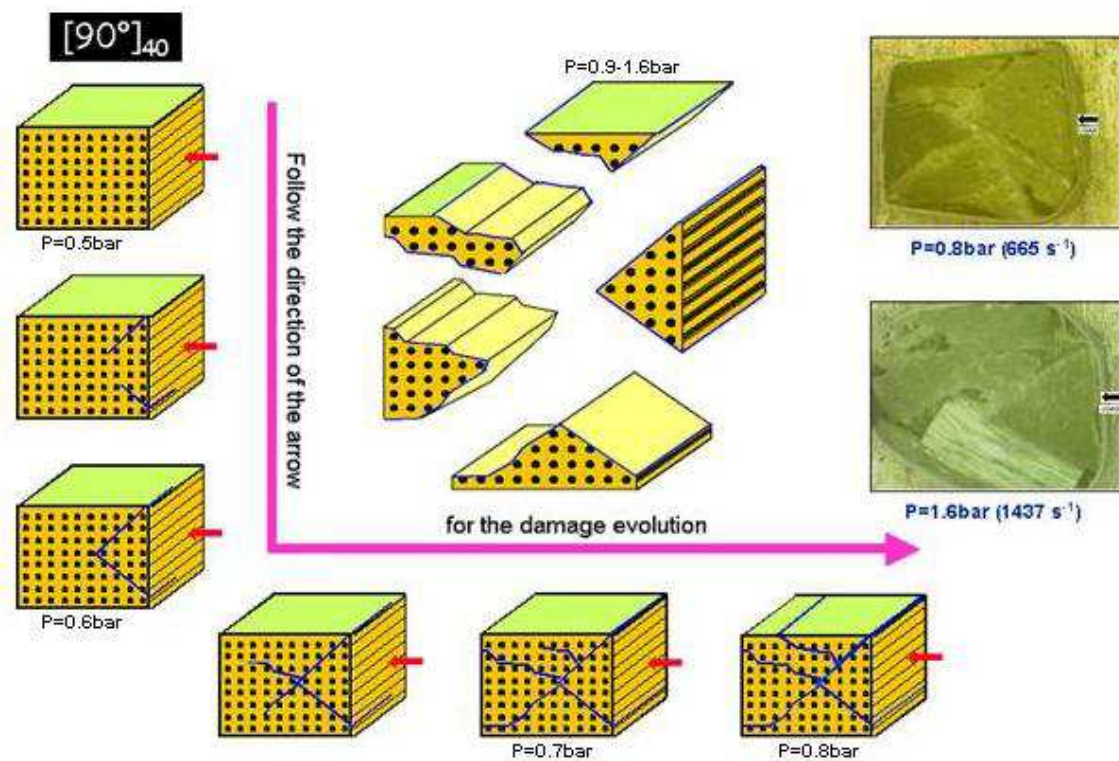


Fig. 21. Damaging modes for IP tests at high impact pressure for  $[90^\circ]_{40}$

### e) For $[90^\circ]_{40}$ laminates

The damage for  $[90^\circ]_{40}$  specimens occurs for an impact pressure higher than 0.6bar ( $\dot{\epsilon} = 587s^{-1}$ ). The damage is initiated by a crack crossing the laminate layers and forming the letter V. The branches of the letter V represent macro cracks, which continue to propagate through the layers. The final failure of the laminate is generated by these cracks. This failure involves the formation of several pieces of various dimensions, Figure 21. There exists a great difference between the damaging modes of  $[0^\circ]_{40}$  and  $[90^\circ]_{40}$ . The failure of  $[90^\circ]_{40}$  is abrupt without delamination or local buckling. The fall in stress is instantaneous.

### 5.2 For out of plane tests

The first observation that one can make, for out-of-plane tests, is that material shows a greater strength. The damage appears only for the great impact pressures: 0.8bar for  $[0^\circ]_{40}$ , 1.4 -1.6bar for ( $[20^\circ]_{20}$  and  $[30^\circ]_{20}$ ) and 1.4bar for  $[45^\circ]_{20}$ . For this lower range of impact pressure there were only residual "plastic" deformations due to matrix cracks. One can also notice that the nature of the damage is strongly affected by the laminates orientation, which stills a parameter in improving also out of plane dynamic compressive strength. The multiplication of the microscopic cracks involves the catastrophic failure. The high strength recorded for  $20^\circ$  and  $30^\circ$  can be correlated with damaging modes observed and reported in figure 22. In fact for these specimens multiple mode fracture is depicted. As the strain rate increase more damage mechanism is involved; from matrix cracking to delamination with multiple paths to final fracture. For  $0^\circ$  and  $45^\circ$  specimens a dominant path is observed along the weakest link, respectively across weft yarns and plies interfaces, which may explain the lower strength. The kinetics of damage for this direction of loading is strongly conditioned by the specimen's fibre orientations. Figures 23 and 24 summarize the history of damaging modes for the various laminates.

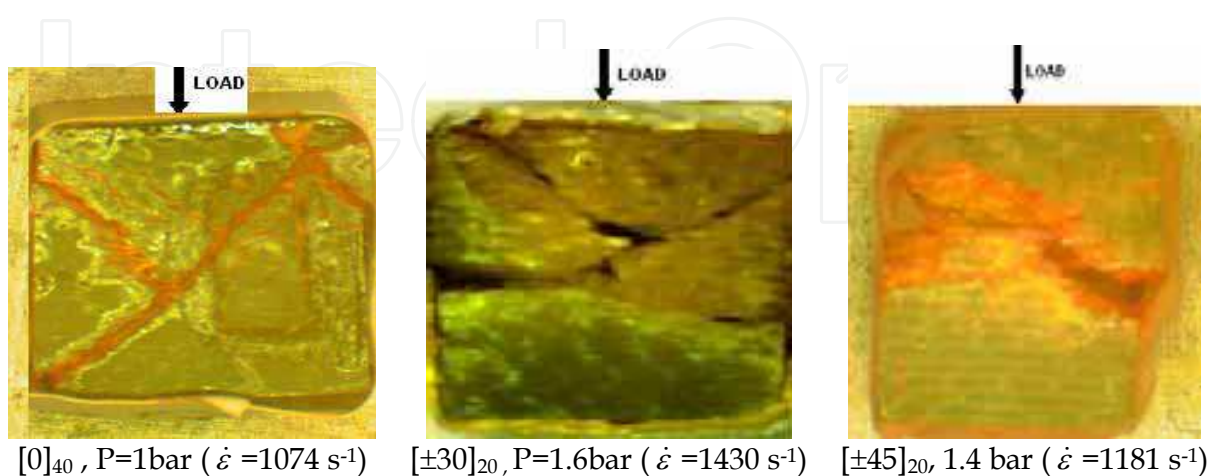


Fig. 22. Damage specimens for out-of-plane tests

<p><math>[0]_{40}</math> <math>[90]_{40}</math></p>		<p>① : Crushing of the resin in contact with the incidental bar                  ② : Formation of damaged zone (V shape)                  ③ : "Macro"-cracks                  ④ : "Micro"-cracks                  ⑤ : Propagation of ② and ③ → Failure</p>
<p><math>[\pm 20]_{20}</math> <math>[\pm 70]_{20}</math></p>		<p>① : Crushing of the resin in contact with the incidental bar                  ② : Layers crushing with plasticity (important crushing in the direction of the incidental bar - matrix cracks)                  ③ : Shearing through the layers - Macro cracks                  ④ : Cracks in the external layers → Failure</p>

Fig. 23. Damage specimens for out-of-plane tests

<p><math>[\pm 30]_{20}</math> <math>[\pm 60]_{20}</math></p>		<p>① : Crushing of the resin in contact with the incidental bar                  ② : Layers crushing with plasticity (important crushing in the direction of the incidental bar - matrix cracks)                  ③ : Shearing through the layers - Macro cracks                  ④ : Cracks in the external layers → Failure</p>
<p><math>[\pm 45]_{20}</math></p>		<p>① : Layers crushing with plasticity                  ② : Micro cracks                  ③ : Macro cracks                  ④ : Propagation of ③ → Failure</p>

Fig. 24. Damaging modes for OP tests

## 6. Conclusions

In this work, the high strain rate material response of  $[0]_{40}$ ,  $[\pm 20]_{20}$ ,  $[\pm 30]_{20}$ ,  $[\pm 45]_{20}$ ,  $[\pm 60]_{20}$ ,  $[\pm 70]_{20}$  and  $[90]_{40}$  E-glass/epoxy composite material systems was investigated. A Split Hopkinson pressure bar was used to conduct high strain rate experiments. Maximum strain rates around  $2000\text{s}^{-1}$  were achieved. Samples were subjected to IP and OP tests. The first observation can be made, for in-plane tests, is that materials show a strength dependency on fibre orientation and impact pressure. Damage appears only for specific impact pressures: 1.2bar for  $[0]_{40}$ , 0.9-1bar for  $([\pm 20]_{20} - [\pm 30]_{20})$ , 0.9bar for  $[\pm 45]_{20}$ , 0.7-0.8bar for  $([\pm 60]_{20} - [\pm 70]_{20})$  and 0.6bar for  $[90]_{40}$ . For this lower range of impact pressure there was no macroscopic damage but the existence of microscopic damage remains a possibility. It can also be noticed that the nature of the damage is strongly affected by the orientation of the laminates, a major parameter in improving dynamic compressive strength. The multiplication of the microscopic and macroscopic damage involves catastrophic failure. For these specimens a multiple fracture mode is determined and described. As the strain rate increases more damage mechanisms are involved; from matrix cracks to delamination with multiple paths to final fracture. The damage kinetics for in-plane loading is strongly conditioned by the specimen's fibre orientations. The initiation and propagation of failure mechanisms at different strain rates have been examined. Specimens fail due to fibre kinking at low strain rates, with delamination and interfacial separation dominating the high strain rate failure regime.

For OP tests, the stress-strain curves of the composite materials show that the material is strongly sensitive to fibre orientation at the same impact pressure: the initial modulus of elasticity and maximum failure stress, strain at maximum stress and the maximum strain are all dependent on fibre orientation and strain rates. The initiation and propagation of failure mechanisms at different strain rates have been examined. The most pronounced effect of increasing the strain rate results in changes in the failure modes. Off-axis composites and angle ply laminates exhibited significant nonlinear and strain dependent behaviour. The glass/epoxy composite material is more resistant for OP loading. Indeed, the damage appears for high pressure.

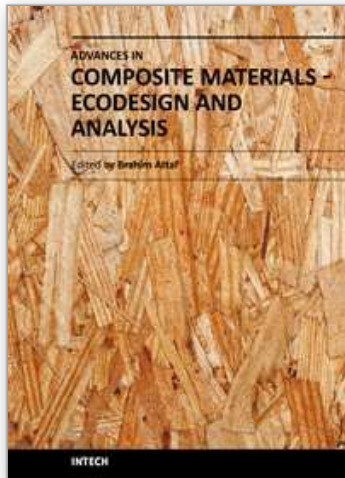
## 7. References

- Bancroft, D. (1941). The velocity of longitudinal waves in cylindrical bars. *Physical Review*, Volume 59, N° 59,1941, 588-593.
- Brara, A. & Klepaczko, J.R. (2007). Fracture energy of concrete at high loading rates in tension. *International Journal of Impact Engineering*, Volume 34, Issue 3, March 2007, 424-435.
- Chamis, C.C. Simplified micromechanics equations for hygral, thermal, and mechanical properties. SAMPE Quarterly, 1984.
- El-Habak A.M.A. (1991). Mechanical behavior of woven glass fiber-reinforced composites under impact compression load. *Composites*, Volume 22, Issue 2, 1991, 129-134.
- Follansbee, P.S. & Frantz, C., (1983). Wave Propagation in the Split Hopkinson Pressure Bar. *Journal of Engineering Materials and Technology*, Volume 105, Issue 1, 61-66.
- Gama, B.A., Gillespie, J.W., Mahfuz, H., Raines, R.P., Haque, A., Jeelani, S., Bogetti, T.A. & Fink, B.K. (2001). High Strain-Rate Behavior of Plain-Weave S-2 Glass/Vinyl Ester Composite. *Journal of Composite Materials*.2001; 35: 1201-1228.

- Gary, G. & Zhao H. (2000). Dynamic testing of fiber polymer matrix composite plates under in-plane compression. *Composites Part A: Applied Science and Manufacturing*, Vol. 31, Issue 8, 2000, 835-840.
- Gilat, A.; Golberg, R.K. & Roberts, G.D. (2002). Experimental study of strain rate dependent behavior of carbon/epoxy composite. *Composite Science and Technology*, 62, 1469-1476 (2002).
- Gillespie, J.W.; Gama B.A.; Cichanowski, C.E. & Xiao, J.R. (2005). Interlaminar shear strength of plain weave S2-glass/SC79 composites subjected to out-of-plane high strain rate compressive loadings. *Composites Science and Technology*, Volume 65, Issues 11-12, September 2005, 1891-1908.
- Goldsmith, W., Dharan, C.K.H. & Chang, H. (1995). Quasi-static and ballistic perforation of carbon fiber laminates. *International Journal of Solids and Structures*, Volume 32, Issue 1, January 1995, 89-103.
- Haque, A. & Ali, M. (2005). High Strain Rate Responses and Failure Analysis in Polymer Matrix Composites - An Experimental and Finite Element Study. *Journal of Composite Materials*, 3 2005; vol. 39: pp. 423 - 450.
- Harding J. (1987). The Effect of High Strain Rate on Material Properties. Materials at High Strain Rate, chapter 4, Ed. T. Z. Blazynski. *Elsevier Applied Science*, London & New York, 1987, 130-173.
- Harding J. (1993). Effect of strain rate and specimen geometry on the compressive strength of woven glass-reinforced epoxy laminates. *Composites*, Volume 24, Issue 4, 1993, 323-332.
- Hosur, M.V.; Alexander, J.; Vaidya, UK.; Jeslani, S. & Mayer A. (2004). Studies on the o-axis high strain rate compression loading of satin weave carbon/epoxy composites. *Computer and Structure* 2004; 63: 75-85.
- Hou, J. P. & Ruiz, C. (2000). Measurement of the properties of woven CFRP T300/914 at different strain rates. *Composites Science and Technology*, Volume 60, Issue 15, November 2000, Pages 2829-2834.
- Kolsky H. (1949). An investigation of the mechanical properties of materials at very high rates of loading. *Proc. Phys. Soc.*, 1949, Vol. 62B, 676-700.
- Kumar P., A. Garg. & Argawal, B.D. (1986). Dynamic compressive behavior of unidirectional GFRP for various fiber orientations. *Material letters*, 1986, Volume 4, Issue 2, 111-116.
- Ochola R. O.; Marcus K.; Nurick G. N. & Franz T. (2004). Mechanical behavior of glass and carbon fiber reinforced composites at varying strain rates. *Composite Structures*, Volume 63, Issues 3-4, February-March 2004, Pages 455-467.
- Ravichandran, G. & Subhash, G, (1994). Critical Appraisal of Limiting Strain Rates for Compression Testing of Ceramics in a Split Hopkinson Pressure Bar. *Journal of the American Ceramic Society*, Volume 77, Issue 1, pages 263-267, January 1994.
- Shi, Y. B.; Hull, D. & Price, J. N (1993). Mode II fracture of + $\theta$ / $-\theta$  angled laminate interfaces. *Composites Science and Technology*, Volume 47, Issue 2, 1993, 173-184.
- Sierakowski R.L. & Nevill G.E. (1971). Dynamic compressive strength and failure of steel reinforced epoxy composites. *Journal of Composite Materials*. 1971, Vol. 5, 362-377.
- Tsai, J.L. & Sun, C.T. (2002). Constitutive model for high strain rate response of polymeric composites. *Composite Science and Technology* 2002;62:1289-97.

- Tsai, J.L. & Sun, C.T. (2004). Dynamic compressive strengths of polymeric composites. *International Journal of Solids and Structures*, Volume 41, Issues 11-12, June 2004, 3211-3224.
- Tsai, J.L. & Sun, C.T. (2005). Strain rate effect on in-plane shear strength of unidirectional polymeric composites. *Composites Science and Technology*, Volume 65, Issue 13, October 2005, 1941-1947.
- Vinson, J.R. & Woldesenbet, E. (2001). Fiber orientation effects on high strain rate properties of graphite/epoxy composites. *Journal of Composite Materials*, 2001, Vol. 35, 509-521.
- Vinson, J.R. & Woldesenbet, E. (2001). Fiber Orientation Effects on High Strain Rate Properties of Graphite/Epoxy Composites. *Journal of Composite Materials*, 3 2001; vol. 35: pp. 509 - 521.
- Zhao, H. & Gary, G., (1996). On the use of SHPB techniques to determine the dynamic behavior of materials in the range of small strains. *International Journal of Solids and structures*, 1996.
- Zukas, J.A., Nicholas, T., Greszczuk, L.B., Swift, H.F., Curran, D.R., (1992). Impact Dynamics, *Wiley*, New York (republished by Krieger, Malabar, FL, 1992).

IntechOpen



## **Advances in Composite Materials - Ecodesign and Analysis**

Edited by Dr. Brahim Attaf

ISBN 978-953-307-150-3

Hard cover, 642 pages

**Publisher** InTech

**Published online** 16, March, 2011

**Published in print edition** March, 2011

By adopting the principles of sustainable design and cleaner production, this important book opens a new challenge in the world of composite materials and explores the achieved advancements of specialists in their respective areas of research and innovation. Contributions coming from both spaces of academia and industry were so diversified that the 28 chapters composing the book have been grouped into the following main parts: sustainable materials and ecodesign aspects, composite materials and curing processes, modelling and testing, strength of adhesive joints, characterization and thermal behaviour, all of which provides an invaluable overview of this fascinating subject area. Results achieved from theoretical, numerical and experimental investigations can help designers, manufacturers and suppliers involved with high-tech composite materials to boost competitiveness and innovation productivity.

### **How to reference**

In order to correctly reference this scholarly work, feel free to copy and paste the following:

Tarfaoui Mostapha (2011). Experimental Investigation of Dynamic Compression and Damage Kinetics of Glass/Epoxy Laminated Composites under High Strain Rate Compression, *Advances in Composite Materials - Ecodesign and Analysis*, Dr. Brahim Attaf (Ed.), ISBN: 978-953-307-150-3, InTech, Available from: <http://www.intechopen.com/books/advances-in-composite-materials-ecodesign-and-analysis/experimental-investigation-of-dynamic-compression-and-damage-kinetics-of-glass-epoxy-laminated-compo>

**INTECH**  
open science | open minds

### **InTech Europe**

University Campus STeP Ri  
Slavka Krautzeka 83/A  
51000 Rijeka, Croatia  
Phone: +385 (51) 770 447  
Fax: +385 (51) 686 166  
[www.intechopen.com](http://www.intechopen.com)

### **InTech China**

Unit 405, Office Block, Hotel Equatorial Shanghai  
No.65, Yan An Road (West), Shanghai, 200040, China  
中国上海市延安西路65号上海国际贵都大饭店办公楼405单元  
Phone: +86-21-62489820  
Fax: +86-21-62489821

© 2011 The Author(s). Licensee IntechOpen. This chapter is distributed under the terms of the [Creative Commons Attribution-NonCommercial-ShareAlike-3.0 License](https://creativecommons.org/licenses/by-nc-sa/3.0/), which permits use, distribution and reproduction for non-commercial purposes, provided the original is properly cited and derivative works building on this content are distributed under the same license.

IntechOpen

IntechOpen